

## Sensitivity of the atmospheric lapse rate to solar cloud absorption in a radiative-convective model

Carynelisa Erlick

Department of Atmospheric Sciences, The Hebrew University of Jerusalem, Jerusalem, Israel

V. Ramaswamy

Geophysical Fluid Dynamics Laboratory, Princeton University, Princeton, New Jersey, USA

Received 19 September 2002; revised 18 March 2003; accepted 22 May 2003; published 29 August 2003.

[1] Previous radiative-convective model studies of the radiative forcing due to absorbing aerosols such as soot and dust have revealed a strong dependence on the vertical distribution of the absorbers. In this study, we extend this concept to absorption in cloud layers, using a one-dimensional radiative-convective model employing high, middle, and low cloud representations to investigate the response of the surface temperature and atmospheric lapse rate to increases in visible cloud absorption. The visible single-scattering albedo (ssa) of the clouds is prescribed, ranging from 1.0 to 0.6, where 0.99 is the minimum that would be expected from the presence of absorbing aerosols within the cloud drops on the basis of recent Monterey Area Ship Track (MAST) Experiment case studies. Simulations are performed with respect to both a constant cloud optical depth and an increasing cloud optical depth and as a function of cloud height. We find that increases in solar cloud absorption tend to warm the troposphere and surface and stabilize the atmosphere, while increases in cloud optical depth cool the troposphere and surface and slightly stabilize the atmosphere between the low cloud top and surface because of the increase in surface cooling. In the absence of considerations involving microphysical or cloud-climate feedbacks, we find that two conditions are required to yield an inversion from a solar cloud absorption perturbation: (1) The solar absorption perturbation must be included throughout the tropospheric clouds column, distributing the solar heating to higher altitudes, and (2) the ssa of the clouds must be  $\leq 0.6$ , which is an unrealistically low value. The implication is that there is very little possibility of significant stabilization of the global mean atmosphere due to perturbation of cloud properties given current ssa values. **INDEX TERMS:** 0345 Atmospheric Composition and Structure: Pollution—urban and regional (0305); 1620 Global Change: Climate dynamics (3309); 3359 Meteorology and Atmospheric Dynamics: Radiative processes; **KEYWORDS:** solar cloud forcing, radiative-convective model, indirect aerosol effect

**Citation:** Erlick, C., and V. Ramaswamy, Sensitivity of the atmospheric lapse rate to solar cloud absorption in a radiative-convective model, *J. Geophys. Res.*, 108(D16), 4522, doi:10.1029/2002JD002966, 2003.

### 1. Introduction

[2] One of the first studies showing the influence of cloud properties on surface temperature and lapse rate was that of *Manabe and Strickler* [1964]. Using a one-dimensional radiative-convective model with a convective adjustment routine, where the critical lapse rate for convective adjustment was  $6.5 \text{ K km}^{-1}$ , they investigated the effect of cloud height on the annual mean thermal equilibrium of the atmosphere. They found that middle and low clouds with moderate solar absorption tend to cool the Earth's surface and increase atmospheric stability, while clouds higher than 9 km altitude with an emissivity greater than 0.5 tend to heat

the surface and decrease atmospheric stability. These results pertain to cloud layers which absorb very little solar radiation, i.e., clouds comprised solely of  $\text{H}_2\text{O}$  condensates.

[3] Studies have also been done on radiative-convective equilibrium in an atmosphere containing solar absorbers, such as smoke and dust aerosols, the so-called "nuclear winter" experiments [*Ramaswamy and Kiehl*, 1985; *Cess et al.*, 1985]. With an aerosol optical depth ranging from 0.2 to 2.0, these aerosol particles create a large heating rate in the troposphere and a large reduction in solar flux at the surface, resulting in a temperature inversion in the troposphere and surface cooling. (An inversion is defined to be a state in which warmer air resides above cooler air, corresponding to a negative lapse rate.) It was found that the strength and vertical extent of the inversion and the amount of surface cooling strongly depend on the single-scattering albedo

(ssa) and vertical distribution of the aerosol particles, specifically on the altitude of maximum solar absorption with respect to the maximum in longwave emission.

[4] The question arises as to which scenario applies in the context of clouds which absorb moderately to strongly in the solar regime, e.g., due to embedded absorbing aerosols. On the basis of two Monterey Area Ship Track (MAST) Experiment case studies, *Erlick et al.* [2001] found that absorbing aerosols, particularly supermicron dust and soot aerosols that nucleate small cloud drops, can decrease the visible single-scattering albedo of clouds from near 1.0 to 0.99. This was accompanied by an increase in visible cloud optical depth by a factor of 1.5 to 3. (Cloud optical depth implies cloud extinction optical depth, unless stated otherwise.) The reduction in single-scattering albedo is similar to the theoretical calculations of *Chylek et al.* [1984] for soot volume fractions ranging from  $10^{-7}$  to  $10^{-4}$ , although from measurements of light absorbing material extracted from cloud drops *Twohy et al.* [1989] estimated a less drastic range of values. On the basis of the MAST simulations, we use 0.99 to mark the bounds of the realistically most polluted scenario. We perform a series of experiments gradually decreasing the cloud single-scattering albedo to the predicted value of 0.99 and below, with respect to both a constant cloud optical depth and an increasing optical depth. We use the simulations to investigate how the perturbation of visible cloud absorption, due to the presence of absorbing aerosols within the cloud drops, affects the partitioning of radiation between the atmosphere and surface and the lapse rate.

[5] Since the cloud optical depth is determined chiefly by large-scale processes and the formation of H<sub>2</sub>O condensates, the runs with constant optical depth can be thought of as representing the influence of aerosol carbon content. As the ssa is decreased, the cloud transitions from that in a remote pristine region to that in a rural region and finally to that typical of more urban and severely polluted regions. Runs with increasing optical depth, on the other hand, may be thought of as representing an increase in H<sub>2</sub>O condensate as a result of a shift in the large-scale system encompassing the cloud.

## 2. Model Description

[6] The RCM is an analog of the three-dimensional Geophysical Fluid Dynamics Laboratory (GFDL) SKYHI GCM (a detailed description of which is given by *Hamilton et al.* [1995]). The model contains 40 vertical levels, with  $\sim 1$  km resolution in the troposphere, increasing to  $\sim 2$  km in the stratosphere and to  $\sim 4$ –5 km in the mesosphere. The latitude-longitude resolution is  $3.0^\circ$  by  $3.6^\circ$ .

[7] For the purposes of this experiment, the model is run in zonally averaged mode. Initial atmospheric temperature and species profiles are taken at latitude  $37.5^\circ\text{N}$  and month June from a 5-year average of SKYHI GCM simulations. Trace gases included in the runs, which are assumed to be uniformly mixed from the surface to the top of the atmosphere, are: CO<sub>2</sub> (337 ppmv), H<sub>2</sub>O, O<sub>3</sub>, CH<sub>4</sub> (1570 ppbv), N<sub>2</sub>O (303 ppbv), CFC-11 (158 pptv), CFC-12 (273 pptv), CFC-113 (23 pptv), and HCFC-22 (62 pptv). Clouds are prescribed at 3 levels, low, middle, and high. The low cloud

is a maximally overlapped cloud with cloud amount 0.269, extending from  $\sim 0.5$  to  $\sim 3.0$  km altitude, with nominal extinction optical depth  $\sim 4.5$  in the visible. The middle cloud is a randomly overlapped cloud with cloud amount 0.07, extending from  $\sim 3.0$  to  $\sim 4.0$  km, with a nominal extinction optical depth  $\sim 3.3$  in the visible. The high cloud is a randomly overlapped cloud with cloud amount 0.159, extending from  $\sim 8.5$  to  $\sim 10$  km, with a nominal extinction optical depth  $\sim 1.1$  in the visible. All clouds have a constant emissivity of 1.0, and no aerosols are (explicitly) included.

[8] In each of the runs, the solar constant is set to  $1370 \text{ W m}^{-2}$ , the surface albedo is set to 0.15, and the astronomy corresponds to the global average (cosine of the solar zenith angle is 0.5, day fraction is 0.5). The shortwave radiation [*Freidenreich and Ramaswamy*, 1999] and longwave radiation [*Schwarzkopf and Fels*, 1991; *Schwarzkopf and Ramaswamy*, 1999] schemes are similar to those in the SKYHI GCM. Convection is simulated with either a Fickian diffusion scheme [*Ramaswamy and Kiehl*, 1985] or a conventional convective adjustment scheme [*Manabe and Wetherald*, 1967]. Finally, relative humidity can either be fixed (allowing for water vapor feedback) or temperature dependent (with fixed specific humidity).

## 3. Results

### 3.1. Fickian Diffusion Scheme With Water Vapor Feedback

#### 3.1.1. Low Clouds Perturbed

[9] We first use the Fickian diffusion scheme to consider the effect of increasing solar absorption in the low cloud layers of the model, where the largest influence of absorbing aerosols on cloud properties is expected in the real atmosphere. In these runs, the low cloud single-scattering albedo is gradually decreased from 1.0 to 0.99, and then as an extreme down to 0.6. As mentioned earlier, 0.99 represents the minimum expected in a severely polluted situation, corresponding to that computed by *Erlick et al.* [2001] for a continentally influenced marine stratocumulus cloud containing dust and soot aerosols. The lower values of 0.8 and 0.6 are used to explore the model sensitivity, and may be considered applicable to the interstitial unactivated aerosol particles in a severely polluted cloud layer. The perturbations occur in the frequency range  $8200$ – $57,600 \text{ cm}^{-1}$ , which is also consistent with the wavelength range of the decreases in cloud ssa computed by *Erlick et al.* [2001]. The cloud ssa values at all other frequencies are left at nominal values, computed using the *Slingo* [1989] parameterization (typical values mentioned in section 2). The properties of the middle- and high-level clouds are left unperturbed at all frequencies.

[10] The equilibrium temperature and lapse rate profiles for a selection of single-scattering albedos are shown in Figures 1a and 1b. Figure 1a shows that the perturbation in cloud ssa down to a value of 0.99 causes only a small increase in temperature at all levels in the troposphere, but no discernible change in lapse rate. As the low cloud ssa is decreased to the extreme value of 0.8, there is a large jump in temperature at all tropospheric levels, but again no change in lapse rate. As the cloud ssa is further decreased to 0.6, the jump in temperature becomes less drastic, as warming from the local solar heating competes against

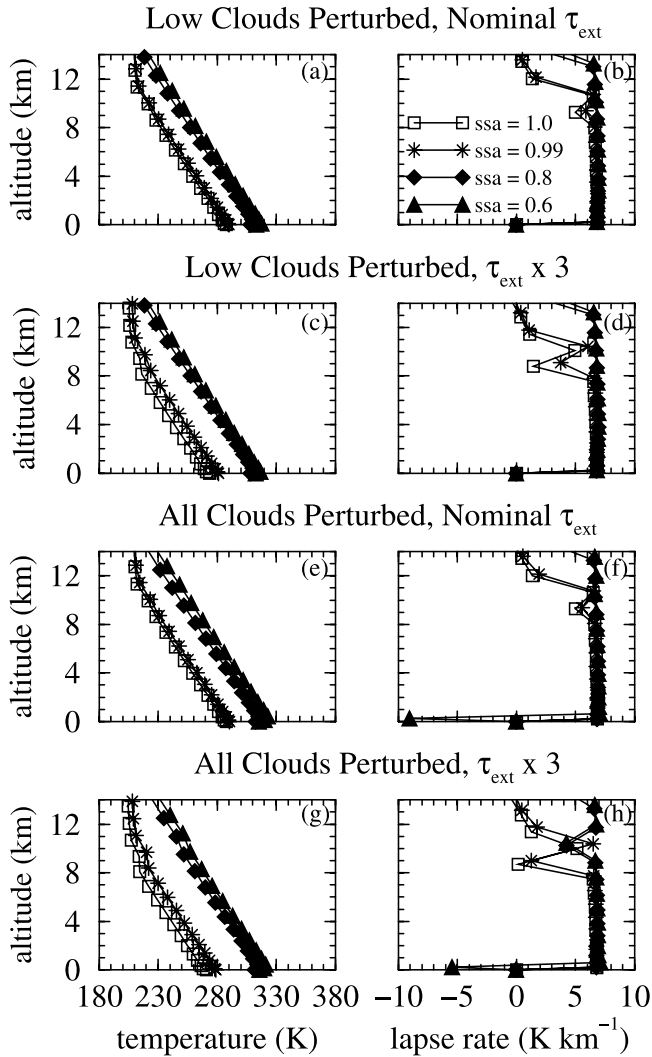


**Figure 1.** (a–h) Temperature (left column) and lapse rate (right column) profiles for a selection of single-scattering albedos (ssa). The four rows of plots represent, respectively: low cloud ssa perturbed with nominal extinction optical depths; low cloud ssa perturbed with low cloud extinction optical depth increased by a factor of 3; all cloud ssa values perturbed with nominal extinction optical depths; all cloud ssa values perturbed with all cloud extinction optical depths increased by a factor of 3.

cooling due to the blocking of radiation from reaching the surface. However, once again there is no discernible change in lapse rate (the actual change in low cloud top to surface lapse rate with respect to  $ssa = 1.0$  is from  $7.15$  to  $5.43 \text{ K km}^{-1}$ ).

[11] In all of these cases, there is efficient coupling between the atmosphere and surface (in the context of this study this is defined to be coupling between the surface and the atmosphere up to 5 or 10 km), and the overall effect is a shift in the temperature profile toward warmer temperatures. This is in the opposite direction to the nuclear winter experiments, in which absorbing aerosols in the atmosphere shift the temperature profile toward cooler temperatures by blocking radiation from reaching the surface [see *Ramaswamy and*

*Kiehl, 1985; Cess et al., 1985*]. The fundamental difference between the solar absorbing aerosols and the solar absorbing clouds is the fraction of sky covered. While the aerosol layer in the nuclear winter experiments is assumed to cover 100% of the sky, the fractional cloud amount (typical values given in section 2) is never 100%. At least 50% of sunlight still reaches the surface unattenuated by clouds, allowing the atmosphere to remain convectively coupled to the surface. As long as the atmosphere is convectively coupled to the surface, the surface warms when heat is deposited into the atmosphere. This is similar to the forcing by solar absorbing aerosols that are distributed inhomogeneously rather than with 100% sky coverage. Such a distribution of solar absorbing aerosols is found to warm the atmosphere and surface [Penner, 1995; Hansen et al., 1997; Schult et al., 1997; Haywood and Ramaswamy, 1998].

[12] In the second set of runs, the perturbations to the low cloud ssa are the same as in the previous set, but the low cloud extinction optical depth is increased by a factor of 3 at all frequencies. This is the maximum increase in cloud optical depth found by *Erlick et al. [2001]* due to the increase in  $\text{H}_2\text{O}$  condensate resulting from the nucleation of continental type aerosols. The equilibrium temperature and lapse rate profiles for a selection of single-scattering albedos from this set of runs are shown in Figures 1c and 1d. The equilibrium temperature of the control run ( $ssa = 1.0$ ) is on the order of 14 degrees cooler than with the nominal cloud optical depth because of the extra reflection back to space. When the low cloud ssa is reduced, the tropospheric temperature increases to the point where at the extreme values of 0.8 and 0.6, the temperature profiles and lapse rates have reverted to their nominal optical depth values (compare with Figure 1a). Although in Figure 1c the low cloud extinction optical depth is higher than in Figure 1a, the absorption optical depth is proportionally higher as well and the net effect is the same as in Figure 1a. For all of these cases, the lower troposphere and surface remain coupled, with the lapse rate between the low cloud top and surface varying from  $7.56$  to  $5.41 \text{ K km}^{-1}$ .

[13] The surface temperatures, radiative fluxes, and lapse rates for the above sets of runs are listed in the first two panels of Table 1 for all values of single-scattering albedo used in the experiment. As was seen in Figure 1, the equilibrium surface temperature ( $T_{\text{sfc}}$ ) gradually increases with decreasing ssa, from 288 K to 313 K for the nominal optical depth (Nominal  $\tau_{\text{ext}}$ ) and from 273 K to 313 K for  $\tau_{\text{ext}} \times 3$ . The net shortwave flux at the TOA ( $F_{\text{sw}}^{\text{net TOA}}$ ) and the outgoing longwave radiation (OLR) are in balance in all cases, gradually increasing from  $230 \text{ W m}^{-2}$  to  $285 \text{ W m}^{-2}$  for nominal optical depth and from  $201 \text{ W m}^{-2}$  to  $284 \text{ W m}^{-2}$  for  $\tau_{\text{ext}} \times 3$ .

[14] The shortwave forcing at the TOA (SW Forcing TOA), defined as the instantaneous change in net shortwave irradiance, ranges up to  $49 \text{ W m}^{-2}$  for the nominal optical depth and up to  $72 \text{ W m}^{-2}$  for  $\tau_{\text{ext}} \times 3$ . (Note that each optical depth has its own control case with the same optical depth but with  $ssa = 1.0$ . All forcings are computed relative to this control possessing the same extinction optical depth.) Forcing within the atmosphere, or the instantaneous change in atmospheric absorption ( $dA_{\text{atm}}$ ), is positive in all

**Table 1.** Radiative Convective Model Results<sup>a</sup>

SSA	T <sub>sfc</sub>	F <sub>sw</sub> <sup>net</sup> TOA	OLR	SW Forcing TOA	dA <sub>atm</sub>	dA <sub>sfc</sub>	-dT/dz <sub>cloud_top</sub>	-dT/dz <sub>low</sub>
<i>Low Cloud SSA Perturbed, Nominal <math>\tau_{ext}</math></i>								
1.0	287.58	229.65	229.70	0.00	0.00	0.00	7.15	6.88
0.999999	287.58	229.65	229.71	0.00	0.00	0.00	7.15	6.88
0.99999	287.58	229.66	229.72	0.01	0.02	-0.01	7.15	6.88
0.9999	287.61	229.72	229.78	0.06	0.13	-0.07	7.15	6.88
0.999	287.87	230.28	230.34	0.51	1.07	-0.55	7.13	6.88
0.99	290.10	235.14	235.20	4.50	9.43	-4.94	6.92	6.87
0.8	308.44	275.73	275.67	40.19	86.14	-45.95	5.68	6.87
0.6	313.25	285.46	285.40	49.34	104.42	-55.08	5.43	6.83
<i>Low Cloud SSA Perturbed, <math>\tau_{ext} \times 3</math></i>								
1.0	273.41	200.97	201.01	0.00	0.00	0.00	7.56	6.81
0.999999	273.41	200.98	201.02	0.01	0.01	0.00	7.56	6.81
0.99999	273.43	201.01	201.06	0.03	0.05	-0.02	7.56	6.81
0.9999	273.53	201.24	201.28	0.21	0.36	-0.15	7.55	6.81
0.999	274.39	203.09	203.14	1.68	2.92	-1.24	7.49	6.81
0.99	281.14	217.73	217.79	13.38	23.24	-9.87	6.93	6.79
0.8	308.43	276.27	276.21	63.93	100.85	-36.92	5.56	6.83
0.6	312.65	284.53	284.47	71.65	109.09	-37.44	5.41	6.81
<i>All Cloud SSA Perturbed, Nominal <math>\tau_{ext}</math></i>								
1.0	287.57	229.61	229.67	0.00	0.00	0.00	7.15	6.88
0.999999	287.57	229.62	229.68	0.00	0.01	0.00	7.15	6.88
0.99999	287.57	229.63	229.69	0.01	0.02	-0.01	7.15	6.88
0.9999	287.61	229.71	229.77	0.07	0.15	-0.08	7.15	6.88
0.999	287.89	230.35	230.41	0.60	1.25	-0.65	7.12	6.88
0.99	290.41	236.03	236.09	5.29	11.06	-5.77	6.89	6.87
0.8	312.72	284.79	284.73	48.50	103.97	-55.48	5.43	6.83
0.6	315.28	297.65	297.54	60.78	129.46	-68.68	3.91	-9.04
<i>All Cloud SSA Perturbed, <math>\tau_{ext} \times 3</math></i>								
1.0	270.98	196.22	196.27	0.00	0.00	0.00	7.64	6.80
0.999999	270.99	196.23	196.28	0.01	0.01	-0.01	7.64	6.80
0.99999	271.00	196.27	196.32	0.04	0.06	-0.02	7.64	6.80
0.9999	271.11	196.51	196.56	0.23	0.40	-0.17	7.63	6.80
0.999	271.97	198.53	198.58	1.86	3.25	-1.40	7.54	6.80
0.99	279.08	214.52	214.58	14.89	26.08	-11.19	6.95	6.78
0.8	311.66	285.30	285.24	76.94	126.33	-49.39	5.32	6.78
0.6	315.64	296.97	296.83	87.98	141.15	-53.18	4.48	-5.46

<sup>a</sup>Here SSA is single-scattering albedo,  $\tau_{ext}$  is cloud extinction optical depth, T<sub>sfc</sub> is equilibrium surface temperature in K, F<sub>sw</sub><sup>net</sup> is net shortwave irradiance in W m<sup>-2</sup>, TOA is top of the atmosphere, OLR is outgoing longwave radiation in W m<sup>-2</sup>, SW Forcing is the instantaneous change in net shortwave irradiance in W m<sup>-2</sup>, dA<sub>atm</sub> is the instantaneous change in atmospheric absorption in W m<sup>-2</sup>, dA<sub>sfc</sub> is the instantaneous change in surface absorption in W m<sup>-2</sup>, and -dT/dz is the lapse rate in K km<sup>-1</sup>.

three sets of runs, and as expected increases with decreasing cloud ssa. Forcing at the surface, or the instantaneous change in surface absorption (dA<sub>sfc</sub>) is negative in all three sets of runs, and as expected also gets larger in magnitude with decreasing cloud ssa. The increase in magnitude, however, is smaller for  $\tau_{ext} \times 3$  than for the nominal optical depth. Here the increase in scattering offsets the potential increase in surface absorption due to the increasing cloud absorption. In effect, for the lowest ssa the absorption in the atmosphere “saturates” as the extinction optical depth increases.

[15] Finally, the lapse rate of temperature is calculated in two ways: both from the top of the low cloud to the surface (-dT/dz<sub>cloud\_top</sub>) and in the lowest atmospheric layer (-dT/dz<sub>low</sub>). For all three sets of runs, the lapse rate calculated from the low cloud top to surface decreases in magnitude (stabilizes) as the low cloud becomes more absorbing, but always remains positive. Note that the lapse rate converges to the similar values for the highest absorption in the two sets of runs, indicating that the lapse rate is insensitive to the extinction optical depth under such strong cloud absorption conditions. The lapse rate in the lowest layer changes very

little for ssa  $\geq 0.99$  and decreases in magnitude minimally from there on.

### 3.1.2. All Clouds Perturbed

[16] To test the sensitivity of the results to cloud height, we repeat the simulations, perturbing all clouds in the same manner as the low clouds. This can be interpreted as simulating the penetration of pollution through the top of the boundary layer such that it perturbs clouds in the free troposphere. The perturbations to ssa again occur in the frequency range 8200–57,600 cm<sup>-1</sup>, and cloud ssa at all other frequencies remain at nominal values. As before, the cloud ssa is gradually decreased from 1.0 to 0.99, and then as an extreme down to 0.6. Equilibrium temperature and lapse rate profiles for the third set of runs where the all cloud ssa is perturbed but the optical depths are held at their nominal values are shown in Figures 1e and 1f. For perturbations in cloud ssa down to 0.8, the results are very similar to Figures 1a and 1c. At ssa = 0.6 an extra feature appears, a small inversion below the low cloud layer with a lapse rate of -9 K km<sup>-1</sup>. Here we have an inversion confined to the lowest atmospheric layer by virtue of having a low-lying maximum in solar absorption.

**Table 2.** Sensitivity to Water Vapor Feedback and Convective Scheme: Maximum Perturbations<sup>a</sup>

	$T_{\text{sfc}}$	SW Forcing TOA	$-dT/dz_{\text{low}}$	Inversion?
<i>Low Cloud SSA Perturbed, Nominal <math>\tau_{\text{ext}}</math></i>				
Fickian diffusion	26	49	-0.05	no
No water vapor feedback	4	49	-0.09	no
Convective adjustment	28	49	0	no
<i>Low Cloud SSA Perturbed, <math>\tau_{\text{ext}} \times 3</math></i>				
Fickian diffusion	39	72	-0.02	no
No water vapor feedback	8	72	-0.06	no
Convective adjustment	42	72	0	no
<i>All Cloud SSA Perturbed, Nominal <math>\tau_{\text{ext}}</math></i>				
Fickian diffusion	28	61	-16	yes
No water vapor feedback	5	61	-0.12	no
Convective adjustment	36	61	0	no
<i>All Cloud SSA Perturbed, <math>\tau_{\text{ext}} \times 3</math></i>				
Fickian diffusion	45	88	-12	yes
No water vapor feedback	8	88	-0.09	no
Convective adjustment	52	88	0	no

<sup>a</sup>Notation is the same as in Table 1, except that the values are now the maximum perturbations in the quantities within the range of experiments rather than the absolute values.

[17] In the fourth set of runs, the perturbations to cloud ssa are the same as in the previous set, but the extinction optical depths of all of the clouds are increased by a factor of 3. Equilibrium temperature and lapse rate profiles for the  $\tau_{\text{ext}} \times 3$  runs are shown in Figures 1g and 1h. The equilibrium temperature of the control run (ssa = 1.0) is on the order of 17 degrees cooler than with the nominal cloud optical depths because of the extra reflection by all of the cloud layers. When the cloud ssa decreases to the extreme values of 0.8 and 0.6, the temperature profiles again revert to values similar to those at nominal optical depth (compare with Figure 1e). As before, although the cloud optical depths are much higher, the absorption optical depths are proportionally higher as well, creating the same net effect as in Figure 1e. The inversion lapse rate at ssa = 0.6 in Figure 1h is  $-5 \text{ K km}^{-1}$ . This is smaller than the inversion at ssa = 0.6 in Figure 1f because the increased optical depth in the high cloud tends to warm the surface and reduces the atmosphere to surface contrast.

[18] The surface temperatures, fluxes, and lapse rates for the third and fourth sets of runs are listed in the third and fourth panels of Table 1. As was seen in the temperature profiles, the equilibrium surface temperature increases with decreasing ssa, from 288 K to 315 K for the nominal optical depth and from 271 K to 316 K for  $\tau_{\text{ext}} \times 3$ . The net shortwave flux at the TOA and the OLR are again in balance in all cases. They gradually increase with decreasing ssa, from  $230 \text{ W m}^{-2}$  to  $298 \text{ W m}^{-2}$  for the nominal optical depth and from  $196 \text{ W m}^{-2}$  to  $297 \text{ W m}^{-2}$  for  $\tau_{\text{ext}} \times 3$ .

[19] The shortwave forcing at the TOA ranges up to  $61 \text{ W m}^{-2}$  for the nominal optical depth and up to  $88 \text{ W m}^{-2}$  for  $\tau_{\text{ext}} \times 3$ . As before, the instantaneous change in atmospheric absorption is positive in all three sets of runs and increases with decreasing cloud ssa, and the instantaneous change in surface absorption is negative in all three sets of runs and gets larger in magnitude with decreasing cloud ssa. Again all forcings are defined with respect to the ssa = 1.0 case possessing the same optical depth. (Here the control is slightly different than in the first two panels, since

ssa = 1.0 refers to all clouds rather than just low clouds. However, this should make a negligible difference.) Finally, lapse rates are given both between the top of the low cloud and the surface and in the lowest atmospheric layer. For all three sets, the lapse rate begins to decrease in magnitude for ssa  $\leq 0.99$  (indicating stabilization), and for ssa = 0.6 the lapse rate in the lowest layer becomes negative indicating the low-level inversion.

### 3.2. Sensitivity to Water Vapor Feedback and the Convective Scheme

[20] The same sets of runs were performed two additional times, once without water vapor feedback, such that the specific humidity was fixed for all of the runs, and once with a convective adjustment routine in place of the Fickian diffusion routine. The results of these runs (maximum perturbations rather than absolute values) are summarized in Table 2. First looking at the results without water vapor feedback, there was a much smaller effect on the surface temperature without water vapor feedback, with a maximum perturbation of 8 K as compared to a maximum perturbation of 45 K with water vapor feedback. The runs without water vapor feedback did not produce an inversion. The maximum perturbation to the lapse rate in the lowest atmospheric layer without water vapor feedback was  $-0.12 \text{ K km}^{-1}$ , while the maximum perturbation with water vapor feedback was  $-16 \text{ K km}^{-1}$ . Generally, we find that the changes in water vapor loading caused by water vapor feedback act to intensify the role of the perturbation. This indicates that indirect aerosol forcing and water vapor changes have to be jointly considered to evaluate the climatic response.

[21] In the second sensitivity study, with the convective adjustment routine in place of the Fickian diffusion scheme (and water vapor feedback on), the changes in surface temperature were similar to but slightly larger than with the Fickian scheme. The maximum perturbation with convective adjustment was 52 K as opposed to 45 K with Fickian diffusion. Despite the similar perturbation to the surface temperature, because the surface balance in the convective adjustment routine did not include explicit latent

or specific heat fluxes, the convective adjustment routine was unable to sustain a low-level inversion. In order to maintain equilibrium when all clouds were perturbed and the ssa was  $\leq 0.6$ , the net longwave flux near the surface instead became negative while the lapse rate remained at the critical value of  $6.5 \text{ K km}^{-1}$ . Therefore there was nearly zero perturbation to the lapse rate in the convective adjustment runs; the increase in solar cloud absorption served only to move the temperature profile as a whole toward higher temperatures. This lack of perturbation to the lapse rate is in agreement with the results of *Cess et al.* [1985], who found a similar effect using a degraded version of their convective adjustment RCM that did not make use of their boundary layer parameterization. In that case, they found no change in the coupling between atmosphere and surface despite their low smoke single-scattering albedo of 0.7.

#### 4. Summary and Conclusions

[22] Using a radiative convective model with no microphysical feedback or feedbacks associated with large-scale condensation (cloud-climate feedbacks), we find that for a given cloud optical depth an increase in solar cloud absorption (decrease in cloud ssa) always warms the troposphere and surface and stabilizes the atmosphere. For a given ssa, on the other hand, an increase in cloud optical depth cools the troposphere and surface and slightly stabilizes the atmosphere between the low cloud top and surface because of the larger surface cooling. In contrast to the soot and dust aerosol forcing viz. the so-called nuclear winter case [*Cess et al.*, 1985], when only low cloud ssa is perturbed there is no low-level inversion in the atmosphere and the atmosphere and surface remain fully coupled. This is connected to the level of maximum emission, which occurs at an altitude of  $\sim 3 \text{ km}$  in the model. Since the low cloud lies below this peak and since it is confined to only a few layers, the maximum in solar heating from the low cloud always lies at or below the level of the maximum in emission. Therefore the greenhouse effect prevents the formation of an inversion when only the low cloud is perturbed. Even for unrealistically low cloud ssa values, since (unlike in the nuclear winter experiments) the fractional cloud amount is never 100%, the amount of sunlight penetrating to the surface allows the atmosphere and surface to remain convectively coupled.

[23] When all clouds are perturbed such that the solar heating is distributed to higher altitudes, the formation of an inversion depends on the single-scattering albedo. If the ssa is greater than 0.6, there is no low-level inversion in the atmosphere because the solar heating is not enough to compensate the cooling of the troposphere by the clouds scattering radiation back to space.

[24] When all clouds are perturbed and the ssa is  $\leq 0.6$ , we obtain a low-level inversion and the atmosphere and surface begin to decouple. This transition value is in agreement with the results of *Cess et al.* [1985], who found no change in the climate sensitivity parameter ( $\lambda$ ) for an aerosol ssa of 0.95, but a lower nonlinear climate sensitivity parameter for a smoke ssa of 0.7. At our cloud ssa of 0.6, much of the incident solar radiation is absorbed in the atmosphere which cools the surface, and the greenhouse effect is too weak to compensate. Therefore an inversion

forms. Since the optical depth of the low cloud is largest, comparable to the *Ramaswamy and Kiehl* [1985] case where the smoke was distributed with a small-scale height, the maximum in solar absorption lies close to the maximum in longwave emission and the inversion is confined to the area in and below the low cloud layer. However, it should be noted such a low ssa (0.6) is an extreme value and not realistic even for even clouds in highly polluted regions, although it might be representative of interstitial unactivated aerosol particles in such polluted environments. We therefore conclude that under the assumption of partial cloud cover of the sky, increases in solar absorption in clouds within the expected range due to absorbing aerosols within the cloud drops do not cause enough stabilization in the atmosphere to form an inversion.

[25] From sensitivity experiments with respect to water vapor feedback and to the type of convection scheme, we find that water vapor feedback is a strong determinant of surface temperature change, indicating its importance for the aerosol-cloud interaction problem. The details of the convective scheme, however, are not particularly relevant.

[26] Assuming the most realistic scenario: only low clouds perturbed, nominal cloud optical depths, and a cloud ssa minimum of 0.99, we calculate a forcing due to solar absorption in clouds of  $4.5 \text{ W m}^{-2}$ . This value is significant in comparison with estimates of the forcings due to greenhouse gases, aerosol direct and indirect effects, and increases in the solar constant [*Ramaswamy et al.*, 2001]. However, this should be taken as more of a regionally defined estimate rather than a global value, since taken globally it would be effectively assuming that all low clouds over the globe were maximally perturbed by absorbing aerosols in their drops. Furthermore, it does not take into account feedback of the perturbation on the cloud amount or cloud microphysical properties. Accounting for such feedback may result in a forcing of lower magnitude or even opposite sign, and should be investigated in the context of a general circulation model.

[27] **Acknowledgments.** Financial support was provided by the Israel Science Foundation, administered by the Israel Academy of Science (grant 153/01). We thank M. D. Schwarzkopf for his assistance with running the RCM.

#### References

- Cess, R. D., G. L. Potter, S. J. Ghan, and W. L. Gates, The climatic effects of large injections of atmospheric smoke and dust: A study of climate feedback mechanisms with one- and three-dimensional climate models, *J. Geophys. Res.*, *90*, 12,937–12,950, 1985.
- Chýlek, P., V. Ramaswamy, and R. J. Cheng, Effect of graphitic carbon on the albedo of clouds, *J. Atmos. Sci.*, *41*, 3076–3084, 1984.
- Erlick, C., L. M. Russell, and V. Ramaswamy, A microphysics-based investigation of the radiative effects of aerosol-cloud interactions for two MAST Experiment case studies, *J. Geophys. Res.*, *106*, 1249–1269, 2001.
- Freidenreich, S. M., and V. Ramaswamy, A new multiple band solar radiative parameterization for GCM's, *J. Geophys. Res.*, *104*, 31,389–31,409, 1999.
- Hamilton, K. P., R. J. Wilson, J. D. Mahlmann, and L. Umscheid, Climatology of the SKYHI troposphere-stratosphere-mesosphere general circulation model, *J. Atmos. Sci.*, *52*, 5–43, 1995.
- Hansen, J., M. Sato, and R. Ruedy, Radiative forcing and climate response, *J. Geophys. Res.*, *102*, 6831–6864, 1997.
- Haywood, J. M., and V. Ramaswamy, Global sensitivity studies of the direct radiative forcing due to anthropogenic sulphate and black carbon aerosols, *J. Geophys. Res.*, *103*, 6043–6058, 1998.
- Manabe, S., and R. F. Strickler, Thermal equilibrium of the atmosphere with convective adjustment, *J. Atmos. Sci.*, *21*, 361–395, 1964.

- Manabe, S., and R. T. Wetherald, Thermal equilibrium of the atmosphere with a given distribution of relative humidity, *J. Atmos. Sci.*, *24*, 241–259, 1967.
- Penner, J. E., Carbonaceous aerosols influencing atmospheric radiation: Black and organic carbon, in *Aerosol Forcing of Climate*, edited by R. J. Charlson and J. Heintzenberg, pp. 91–108, John Wiley, New York, 1995.
- Ramaswamy, V., and J. T. Kiehl, Sensitivities of radiative forcing due to large loadings of smoke and dust aerosols, *J. Geophys. Res.*, *90*, 5597–5613, 1985.
- Ramaswamy, V., O. Boucher, J. Haigh, D. Hauglustaine, J. Haywood, G. Myhre, T. Nakajima, G. Y. Shi, and S. Solomon, Radiative forcing of climate change, in *Climate Change 2001: The Scientific Basis*, edited by J. T. Houghton et al., pp. 349–416, Cambridge Univ. Press, New York, 2001.
- Schult, I., J. Feichter, and W. F. Cooke, Effect of black carbon and sulphate aerosols on the Global Radiation Budget, *J. Geophys. Res.*, *102*, 30,107–30,117, 1997.
- Schwarzkopf, M. D., and S. B. Fels, The simplified exchange method revisited: An accurate, rapid method for computation of infrared cooling rates and fluxes, *J. Geophys. Res.*, *96*, 9075–9096, 1991.
- Schwarzkopf, M. D., and V. Ramaswamy, Radiative effects of CH<sub>4</sub>, N<sub>2</sub>O, halocarbons and the foreign-broadened H<sub>2</sub>O continuum: A GCM experiment, *J. Geophys. Res.*, *104*, 9467–9488, 1999.
- Slingo, A., A GCM parameterization for the shortwave radiative properties of water clouds, *J. Atmos. Sci.*, *46*, 1419–1427, 1989.
- Twohy, C. H., A. D. Clarke, S. G. Warren, L. F. Radke, and R. J. Charlson, Light-absorbing material extracted from cloud droplets and its effect on cloud albedo, *J. Geophys. Res.*, *94*, 8623–8631, 1989.
- 
- C. Erlick, Department of Atmospheric Sciences, The Hebrew University of Jerusalem, Jerusalem 91904, Israel. (caryn@dina.es.huji.ac.il)
- V. Ramaswamy, Geophysical Fluid Dynamics Laboratory, Princeton University, Forrestal Campus, U.S. Route 1, Princeton, NJ 08542, USA. (vr@gfdl.noaa.gov)